Higher Order Impedance Boundary Condition with Integral Method for the Scattering Problem in Electromagnetism

Christian Daveau, Molka Kacem, Soumaya Oueslati, Stefan Bornhofen, and Brice Naisseline
Department of Mathematics, University CY Cergy Paris, Cergy-Pontoise, France

Abstract— In this paper, we implement the high order boundary condition (HOIBC) in the integral equations to solve the scattering problem. We study the HOIBC operators that appear in the boundary integral equations and we propose a discretization of these operators in spaces $H(div)$ and $H(curl)$. Then, we give validations of the HOIBC by calculating the radar cross section (RCS), that show the improvement in accuracy over the standard impedance boundary condition (SIBC). The computation code implements the H-matrix approach with Adaptive Cross Approximation (ACA) and MPI parallelization.

1. INTRODUCTION

The broad objective of this work is to solve time-harmonic scattering problems using the integral method. We consider a coated perfectly conducting closed objects (PEC) to solve Maxwell's equation in the harmonic regime. The method of integral equations is often used to calculate the far field radiated by a homogeneous object since it reduces drastically the number of unknowns compared to other finite elements methods where thin coatings is meshed. It is important to model the finite conductivity of the metal by an impedance boundary condition. This impedance boundary condition defines a relationship between the tangential electric and magnetic fields on a surface. In the paper [6], the author propose a HOIBC which involve at most a first derivative of the field.

In this paper, we present the implementation of the HOIBC in the EFIE and MFIE to improve the accuracy of Leontovich impedance boundary condition proposed in [6]. Then, we develop the problems raised by the discretization of surface *div* and surface *curl* operators involved in the boundary integral equation.

2. IMPEDANCE BOUNDARY CONDITION AND INTEGRAL EQUATIONS

The high order impedance boundary condition is derived using the spectral domain approach, we present the high order impedance boundary condition relating the tangential components of the electric and magnetic fields proposed by [6]:

$$(I + b_1 L_D - b_2 L_R)\mathbf{E}_{tg} = (a_0 I + a_1 L_D - a_2 L_R)(\mathbf{n} \times \mathbf{H}) \tag{1}$$

The unknown coefficients appearing in the polynomial approximation (1) depends on the characteristics of the coating (layer thickness, relative electric permittivity ϵ and magnetic permeability μ).

Aiming for boundary integral equations, we used the representation integral formula for solutions of the electromagnetic problem [2]. We rewrite the impedance boundary condition introduced earlier as a link between the current densities $\mathbf{J}$ and $\mathbf{M}$ and we implement it in the integral representation. We get the expression of the electromagnetic field in terms of the equivalent currents and charges in integral form, known as the Electric Field Integral Equation (EFIE) and the Magnetic Field Integral Equation (MFIE) respectively:

$$E^{inc} = \mathbb{S}\mathbf{J} + \mathbb{D}\mathbf{M} + \frac{1}{2} n \times \mathbf{M} \tag{2}$$

and

$$H^{inc} = \frac{1}{\eta^2}\mathbb{S}\mathbf{M} - \mathbb{D}\mathbf{J} - \frac{1}{2} n \times \mathbf{J} \tag{3}$$

where $\mathbb{S}$ is the single layer operator, $\mathbb{D}$ is the double layer operator and $G(x, y)$ is the Green kernel giving the outgoing solutions to the scalar Helmholtz equation.

By implementing the HOIBC into EFIE and MFIE respectively, we obtain the bilinear form:

$$\begin{aligned}
A(\mathbf{U},\mathbf{\Psi}) \;=\; & \langle \mathbb{S}\mathbf{J}, \mathbf{\Psi}_J\rangle + \frac{1}{\eta^2}\langle \mathbb{S}\mathbf{M}, \mathbf{\Psi}_M\rangle \\
& + \frac{a_2}{2}\langle \nabla_\Gamma\nabla_\Gamma\cdot(n\times\mathbf{J}), n\times\mathbf{\Psi}_J\rangle - \frac{b_1}{2}\langle \nabla_\Gamma\nabla_\Gamma\cdot(n\times\mathbf{M}), \mathbf{\Psi}_J\rangle \\
& + \frac{b_2}{2}\langle \nabla_\Gamma\nabla_\Gamma\cdot\mathbf{M}, n\times\mathbf{\Psi}_J\rangle + \frac{b_1}{2a_0}\langle \nabla_\Gamma\nabla_\Gamma\cdot(n\times\mathbf{M}), n\times\mathbf{\Psi}_M\rangle \\
& + \frac{b_2}{2a_0}\langle \nabla_\Gamma\nabla_\Gamma\cdot\mathbf{M}, \mathbf{\Psi}_M\rangle - \frac{a_1}{2a_0}\langle \nabla_\Gamma\nabla_\Gamma\cdot\mathbf{J}, n\times\mathbf{\Psi}_M\rangle \\
& - \langle \mathbb{D}\mathbf{M}, \mathbf{\Psi}_J\rangle + \langle \mathbb{D}\mathbf{J}, \mathbf{\Psi}_M\rangle + \frac{a_0}{2}\langle \mathbf{J}, \mathbf{\Psi}_J\rangle \\
& + \frac{1}{2a_0}\langle \mathbf{M}, \mathbf{\Psi}_M\rangle + \frac{a_1}{2}\langle \nabla_\Gamma\nabla_\Gamma\cdot\mathbf{J}, \mathbf{\Psi}_J\rangle \\
& + \frac{a_2}{2a_0}\langle \nabla_\Gamma\nabla_\Gamma\cdot(n\times\mathbf{J}), \mathbf{\Psi}_M\rangle .
\end{aligned}$$

Finally, we have the variational formulation: find $\mathbf{U} = (\mathbf{J}, \mathbf{M})$ such that

$$A(\mathbf{U},\mathbf{\Psi}) = F(\mathbf{\Psi}) \tag{4}$$

for all $\mathbf{\Psi} = (\mathbf{\Psi}_J, \mathbf{\Psi}_M)$. Where

$$F(\mathbf{\Psi}) = \int_\Gamma \mathbf{E}^{inc}\cdot\mathbf{\Psi}_J ds + \int_\Gamma \mathbf{H}^{inc}\cdot\mathbf{\Psi}_M ds.$$

In the next section, we will develop a discretization of currents that allow to calculate the components of surface vector in $H(div)$ from those of same vector in $H(curl)$.

3. DISCRETIZATION OF OPERATORS

3.1. FEM

We propose a technique to discretize the HOIBC operators obtained from the variational formulation (4), called the finite element method (FEM). The numerical results obtained after implementation parallel Hierarchical matrices adaptive cross approximation are given in the next section.

The currents $\mathbf{J}$ and $\mathbf{M}$ are discretized with the standard base of Rao-Wilton-Glisson basis functions $\{\mathbf{f}_i\}_{i=1,Ne} \in H(div)$, where each function correspond to one edge:

$$\mathbf{J}(x) = \sum_{i=1}^{Ne} J_i\mathbf{f}_i(x), \quad \mathbf{M}(x) = \sum_{i=1}^{Ne} M_i\mathbf{f}_i(x).$$

As $\mathbf{J}$,$\mathbf{M} \in H(div)$, the operators arising in the discretization of the HOIBC that have $(n\times\mathbf{J})$, $(n\times\mathbf{M}) \in H(curl)$ in the integral are not easily computed, it adds junctions issues. The surface RWG is discontinuous when crossing the edge that borders the two elements on which they are defined. The gradient of the surface divergence of RWG goes to infinity on the edges of the two elements, as does their surface *curl*. It gives us Dirac function on the edges of the two elements. And the surface defined by the mesh does not have continuous first order derivatives.

3.2. Discretization

In the following, we will detail the evaluation of HOIBC operators resulting from the discretization of the variational problem, we begin by the operator D:

$$D_{ij} = \langle \nabla_\Gamma\nabla_\Gamma\cdot\mathbf{f}_j, \mathbf{f}_i\rangle \tag{5}$$

Before explicitly evaluating this operator, we define the formula of theory of distribution:

$$\nabla f = \{\nabla f\} - S_\gamma([f\nu]) \tag{6}$$

Therefore, we use the jump formula and the formula above (6) to overcome the difficulty of the discretization. We get

$$D_{ij} = \int_{\Gamma_h} \nabla_\Gamma\nabla_\Gamma\cdot\mathbf{f}_j\cdot\mathbf{f}_i\, ds = [\nabla_\Gamma\cdot\mathbf{f}_j]_{/i}$$

However, this technique does not work in the evaluation of the other operators that appears in the formulation:

$$F_{ij} = \langle \nabla_\Gamma \nabla_\Gamma \cdot (n \times \mathbf{f}_j), \mathbf{f}_i \rangle \tag{7}$$
$$E_{ij} = \langle \nabla_\Gamma \nabla_\Gamma \cdot \mathbf{f}_j, n \times \mathbf{f}_i \rangle \tag{8}$$
$$G_{ij} = \langle \nabla_\Gamma \nabla_\Gamma \cdot (n \times \mathbf{f}_j), n \times \mathbf{f}_j \rangle \tag{9}$$

For this reason, we express these operators in terms of the operator D by performing the projection from $H(div)$ to $H(curl)$. Hence, we express $\mathbf{f}_i$ in $H(curl)$ basis which is $(-n \times \mathbf{f}_l)_{l=1,Ne}$ to simplify the discretization of these operators.

3.3. Projection from $H(div)$ to $H(curl)$

We rewrite the RWG basis functions as a combination of the basis functions in $H(curl)$ as following:

$$\mathbf{f}_i = \sum_{j=1}^{Ne} c_j^i \widetilde{\mathbf{f}}_j, \tag{10}$$

where $(c_j^i)_{i,j=1,Ne}$ are the components of function $\mathbf{f}_i$ in $\widetilde{\mathbf{f}}_j \in H(curl)$. We consider these components as the unknown coefficients of the projection matrix denoted by $[P]$.

In order to express our problem in matrix form, we multiply $\mathbf{f}_i$ with $\mathbf{q}_i \in H(curl)$ which is the basis proposed in [3] and integrate on the surface Γ:

$$\int_{\Gamma_h} \mathbf{f}_i \cdot q_l \, ds = \sum_{j=1}^{N} c_j^i \int_{\Gamma_h} \widetilde{\mathbf{f}}_j \cdot q_l \, ds. \tag{11}$$

Then, we define the integrals obtained in the expression above:

$$CH_{ij} = \int_{\Gamma_h} q_i \cdot \widetilde{\mathbf{f}}_j \, ds, \quad CK'_{ij} = \int_{\Gamma_h} q_i \cdot \mathbf{f}_j \, ds \tag{12}$$

From the expressions (11) and (12), we derive the projection matrix in a matrix form:

$$[P] = [CH]^{-1}[CK'] \tag{13}$$

Now, we will rewrite the operator F in terms of the operator D as follows:

$$F_{ij} = \int_{\Gamma_h} \nabla_\Gamma \nabla_\Gamma \cdot (n \times \mathbf{f}_j) \cdot \mathbf{f}_i \, ds$$

First, we apply the expression (10) that relates $\mathbf{f_i}$ to $\widetilde{\mathbf{f}}_\mathbf{j}$:

$$F_{ij} = \sum_{k=1}^{Ne} c_k^j \int_{\Gamma_h} \nabla_\Gamma \nabla_\Gamma \cdot (n \times \widetilde{\mathbf{f}}_k) \cdot \mathbf{f_i} \, ds$$

Then, applying the projection properties from $H(div)$ in $H(curl)$ yields:

$$F_{ij} = \sum_{k=1}^{Ne} c_k^j \int_{\Gamma_h} \nabla_\Gamma \nabla_\Gamma \cdot \mathbf{f}_k \cdot \mathbf{f_i} \, ds$$

Using the matrix definition (13) of $[P]$, we get the operator F in a matrix form as follows:

$$[F] = [CH]^{-1}[CK'][D] = [P][D] \tag{14}$$

We reason with the same way for the operator G we get:

$$[G] = [P]^T[D][P] \tag{15}$$

4. NUMERICAL VALIDATIONS

The current section describes the methods applied with a view to meeting both challenges via memory compression and parallel computing. We implemented these methods through an adapted version of the open-source HACApK library for CPU clusters which is originally designed for real-valued BEM-matrices only. Due to the independence of the blocks, H-matrix computing can be conveniently coupled with parallel computing technologies to distribute the memory load, and to accelerate not only the matrix filling but also the classical matrix/vector product in order to obtain fast iterative solvers. The partial multiplications are broadcasted among the MPI processes and added up to the final product.

Now, we will present some numerical results.As a first example, we consider the case of a coated conducting sphere with a conductor radius of $1.5\lambda_0$ and coating thickness of $0.0075\lambda_0$, with $\epsilon_r = 5$

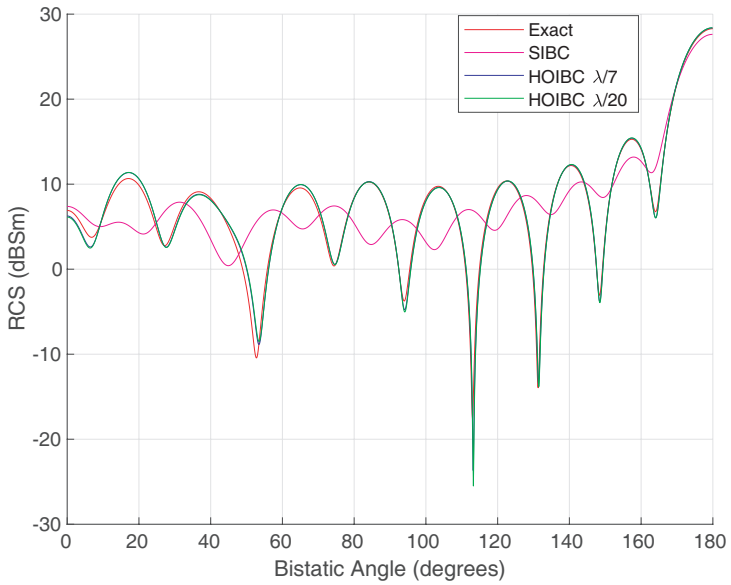

Figure 1: $\theta\theta$ component of the bistatic RCS for a coated conducting sphere with frequency $f = 0.45\,\mathrm{GHz}$, layer thickness $d = 0.05\,\mathrm{m}$, $\varepsilon_r = 5$ and $\mu_r = 1$. Exact serie solution and HOIBC solution.

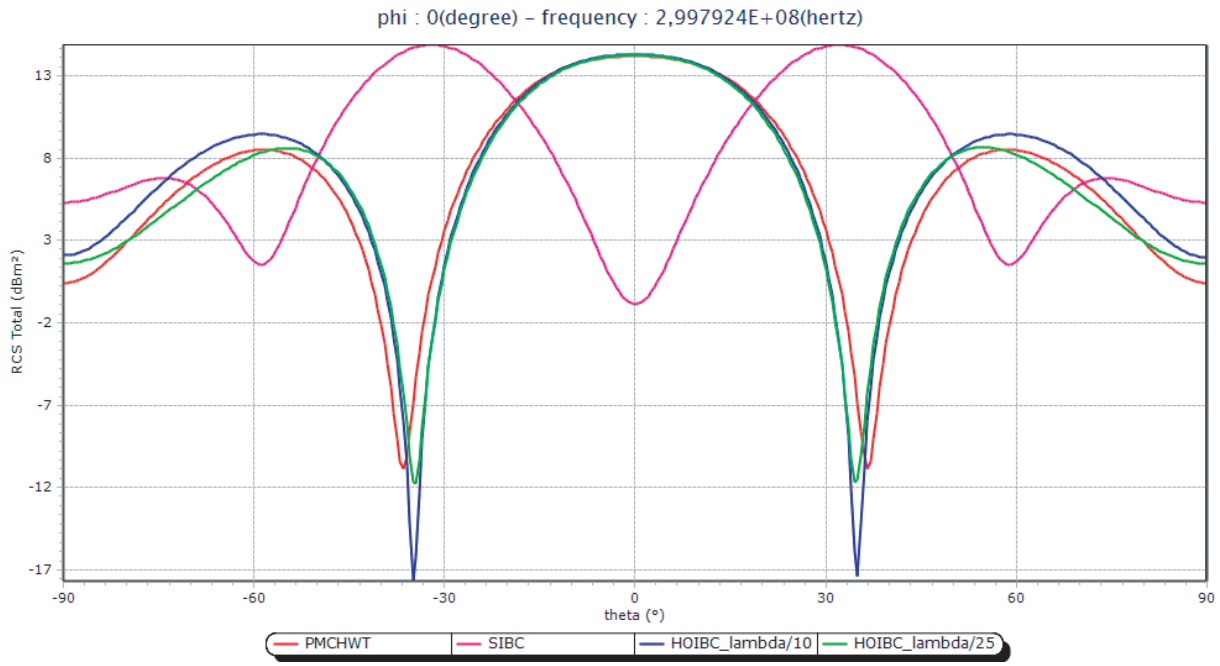

Figure 2: $\theta\theta$ component of the monostatic RCS for a coated conducting spheroid, PMCHWT solution, SIBC solution and HOIBC solution.

and $\mu_r = 1.0$. Figure 1 show the $\theta\theta$ components of the bistatic RCS for a plane wave incident from $\theta = 0$. Three solutions are included: the exact serie solution (MIE) and the solutions of the methods of moment studied below with SIBC and the HOIBC. The Figure clearly shows the increased accuracy of the HOIBC solution relative to the SIBC solution. The SIBC gives only the average behavior of the scattered field while the HOIBC accurately predicts the sidelobe behavior.

The second test is a coated conducting spheroid whose the radii are 0.5 m and 1 m with a coating thickness of $0.17\lambda_0$, with $\epsilon_r = 5$ and $\mu_r = 1.0$. Figures 2 and 3 show the $\theta\theta$ and $\phi\phi$ components of the monostatic RCS. Three solutions are included: a method of moments solution called PMCHWT, the HOIBC solution and the SIBC solution. It does not exits exact solution for this case. We note

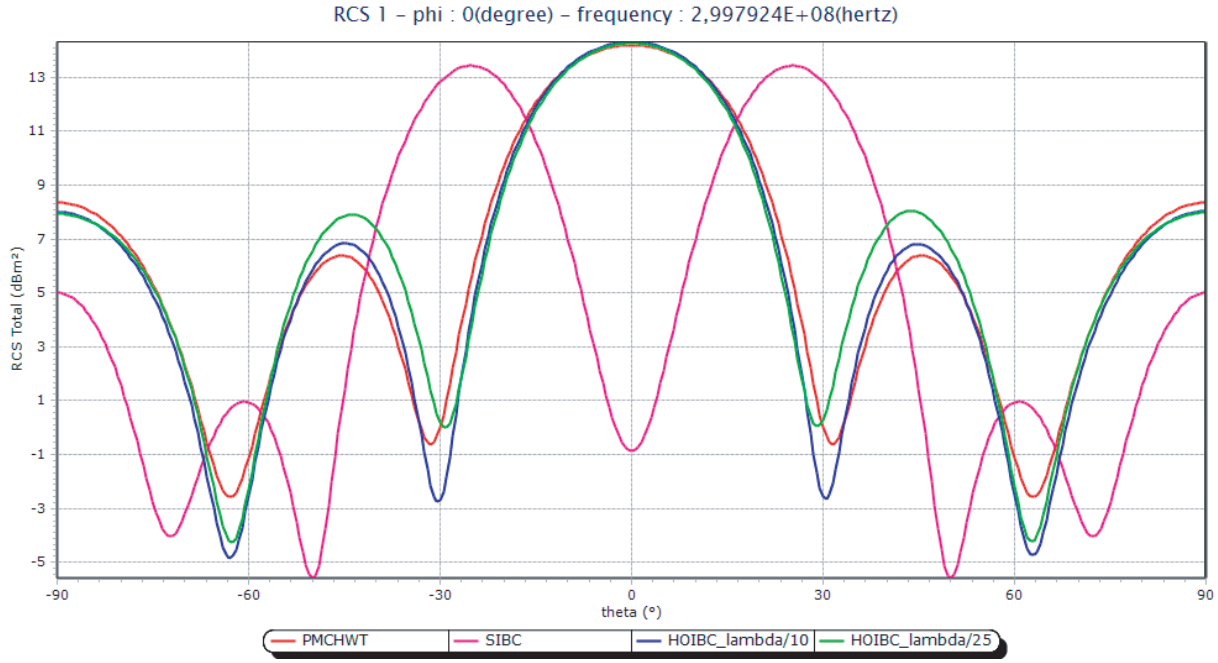

Figure 3: $\phi\phi$ component of the monostatic RCS for a coated conducting spheroid, PMCHWT solution, SIBC solution and HOIBC solution.

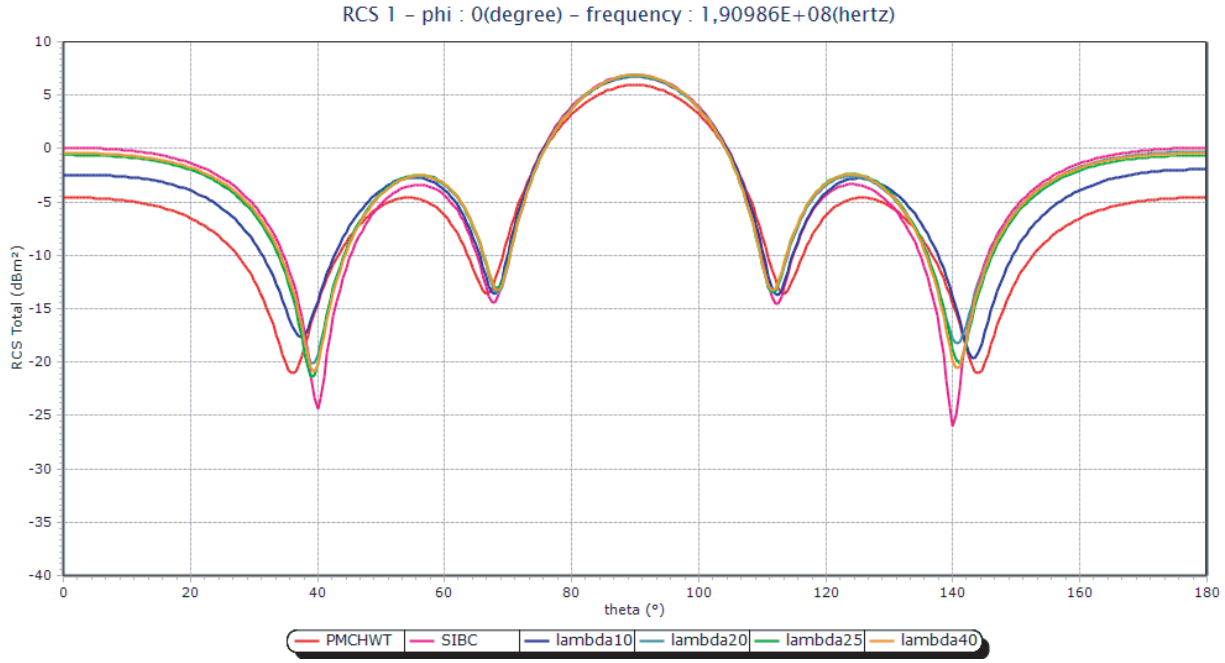

Figure 4: $\phi\phi$ component of the monostatic RCS for a coated conducting cylinder, PMCHWT solution, SIBC solution and HOIBC solution.

that a slight difference between the PMCHWT solution and the HOIBC solution and the SIBC solution is very poor. In both cases, excellent results are obtained for all angles of incidence. But, the finite radii of curvature on the spheroid contribute to the inaccuracy of the HOIBC result.

The third test is a coated conducting cylinder whose the radii are 0.25 m and 2 m with a coating thickness of 0.05 m, with $\epsilon_r = 1 - i$ and $\mu_r = 1.0$. Figure 4 $\phi\phi$ components of the monostatic RCS. Three solutions are included: a method of moments solution called PMCHWT, the HOIBC solution and the SIBC solution. It does not exits exact solution for this case. We note that a slight difference between the PMCHWT solution and the HOIBC solution and the SIBC solution is very poor. In both cases, excellent results are obtained for all angles of incidence. But, the finite radii

Figure 5: $\phi\phi$ component of the monostatic RCS for a coated conducting almond, PMCHWT solution, SIBC solution and HOIBC solution.

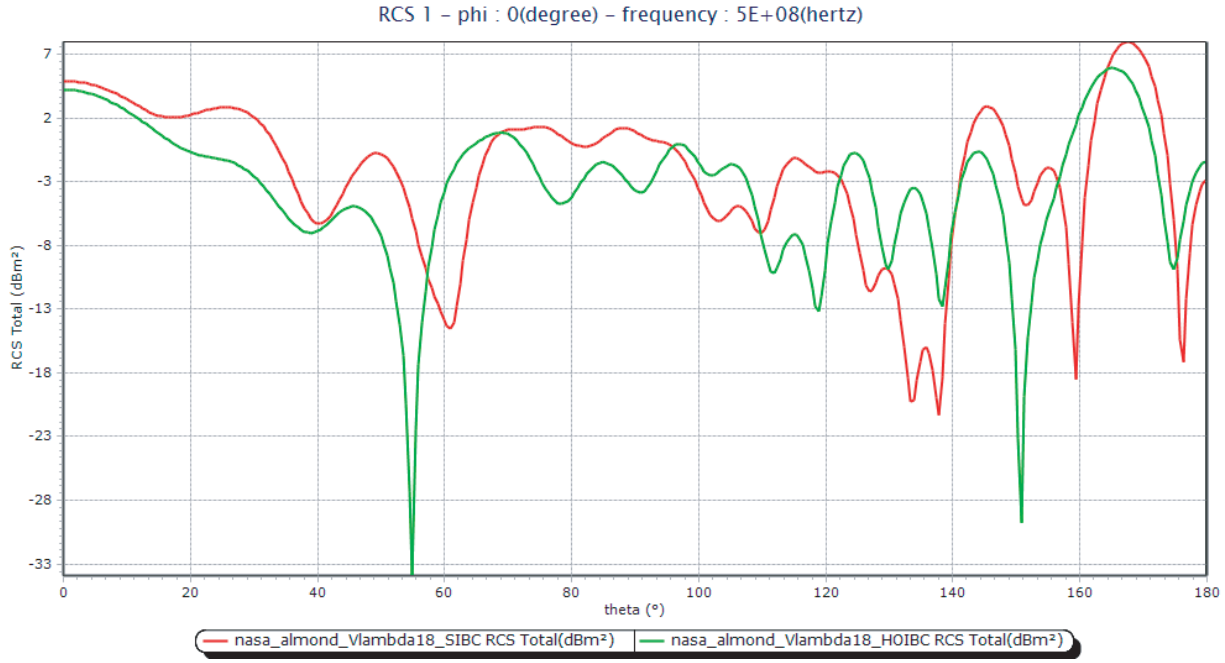

Figure 6: $\theta\theta$ component of the monostatic RCS for a coated conducting almond, PMCHWT solution, SIBC solution and HOIBC solution.

of curvature on the spheroid contribute to the inaccuracy of the HOIBC result.

The fourth test is a coated conducting almond whose the radii are 0.25 m and 2 m with a coating thickness of 0.03 m, with $\epsilon_r = 4$ and $\mu_r = 1.0$.

The fifth test is a coated conducting cone whose the radii are 0.25 m and 2 m with a coating thickness of 0.034 m, with $\epsilon_r = 5$ and $\mu_r = 1.0$.

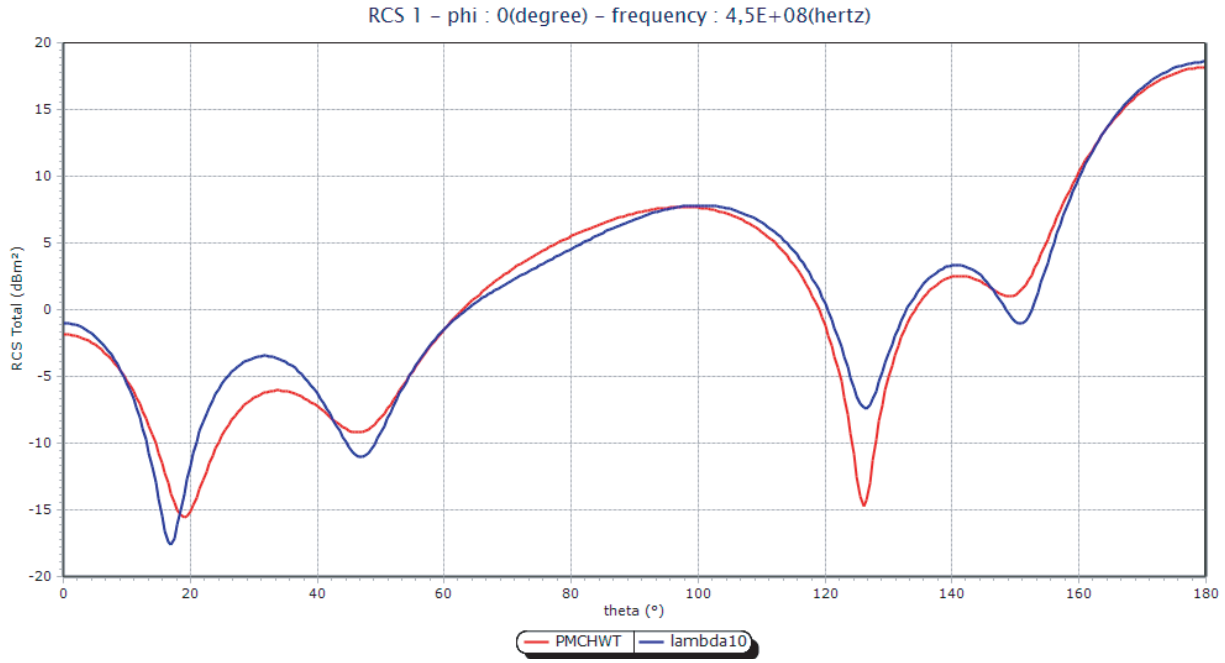

Figure 7: $\theta\theta$ component of the monostatic RCS for a coated conducting cone, PMCHWT solution, SIBC solution and HOIBC solution.

5. CONCLUSION

The implementation of a HOIBC model in a 3D MoM code using RWG basis functions has been presented. We have also developed a computation code to reduce programming costs for parallel the matrix of the HOIBC. The numerical results haves shown an important accuracy improvement of the HOIBC model over a SIBC model in the case of thin layers. The performances of the HOIBC are evaluated by calculating the radar cross section with different meshes.

REFERENCES

1. Y. Rahmat-Samii and D. J. Hoppe, *Impedance Boundary Conditions in Electromagnetics*, Taylor & Francis, 1995.
2. Hsiao, G. C. and R. F. Kleinman, "Mathematical foundations for error estimations in numerical solutions of integral equations in electromagnetics," *IEEE Trans. Antennas Propagat.*, Vol. 45, 316–328, Mar. 1997.
3. Bendali, A., M. Fares, and J. Gay, "A boundary-element solution of the leontovich problem," *IEEE Trans. Antennas Propagat.*, Vol. 47, 1597–1605, Oct. 1999.
4. Bebendorf, M., "Approximation of boundary element matrices," *Numerische Mathematik*, Vol. 86, 565–589, 2000.
5. Aubakirov, A., P. Soudais, and C. Daveau, "High order impedance boundary condition for MoM scattering," *IEEE Symposium on Antennas and Propagation*, Orlando Florida, USA, 2013.
6. Aubakirov, A., *Electromagnetic Scattering Problem with Higher Order Impedance Boundary Conditions and Integral Methods*, UCP, 2014.
7. Oueslati, S., "A new variational formulation for electromagnetic scattering problem using integral method with high order impedance boundary condition — Small perturbations of an interface for Stokes system," CYU University, 2019.